JOURNAL OF VIROLOGY, Nov. 2002, p. 10980–10993 Vol. 76, No. 21
0022-538X/02/$04.00+0 DOI: 10.1128/JVI.76.21.10980–10993.2002
Copyright © 2002, American Society for Microbiology. All Rights Reserved.

Phosphorylation by the Varicella-Zoster Virus ORF47 Protein Serine Kinase Determines whether Endocytosed Viral gE Traffics to the *trans*-Golgi Network or Recycles to the Cell Membrane

T. K. Kenyon,[1] Jeffrey I. Cohen,[2] and Charles Grose[1]*

Department of Microbiology, University of Iowa, Iowa City, Iowa 52242,[1] and Medical Virology Section, Laboratory of Clinical Investigation, National Institute of Allergy and Infectious Diseases, Bethesda, Maryland 20892[2]

Received 30 April 2002/Accepted 3 July 2002

Like all alphaherpesviruses, varicella-zoster virus (VZV) infection proceeds by both cell-cell spread and virion production. Virions are enveloped within vacuoles located near the *trans*-Golgi network (TGN), while in cell-cell spread, surface glycoproteins fuse cells into syncytia. In this report, we delineate a potential role for serine/threonine phosphorylation of the cytoplasmic tail of the predominant VZV glycoprotein, gE, in these processes. The fact that VZV gE (formerly called gpI) is phosphorylated has been documented (E. A. Montalvo and C. Grose, Proc. Natl. Acad. Sci. USA 83:8967-8971, 1986), although respective roles of viral and cellular protein kinases have never been delineated. VZV ORF47 is a viral serine protein kinase that recognized a consensus sequence similar to that of casein kinase II (CKII). During open reading frame 47 (ORF47)-specific in vitro kinase assays, ORF47 phosphorylated four residues in the cytoplasmic tail of VZV gE (S593, S595, T596, and T598), thus modifying the known phosphofurin acidic cluster sorting protein 1 domain. CKII phosphorylated gE predominantly on the two threonine residues. In wild-type-virus-infected cells, where ORF47-mediated phosphorylation predominated, gE endocytosed and relocalized to the TGN. In cells infected with a VZV ORF47-null mutant, internalized VZV gE recycled to the plasma membrane and did not localize to the TGN. The mutant virus also formed larger syncytia than the wild-type virus, linking CKII-mediated gE phosphorylation with increased cell-cell spread. Thus, ORF47 and CKII behaved as "team players" in the phosphorylation of VZV gE. Taken together, the results showed that phosphorylation of VZV gE by ORF47 or CKII determined whether VZV infection proceeded toward a pathway likely involved with either virion production or cell-cell spread.

Varicella-zoster virus (VZV), an alphaherpesvirus, displays a highly cell-associated phenotype in tissue culture; that is, VZV infection spreads from VZV-infected cells to uninfected cells with little or no extracellular virion production. Other alphaherpesviruses do not share this tissue culture phenotype (45). Because VZV is highly cell associated, viral mutant creation requires a cosmid system containing the entire VZV Oka genome, which can then be manipulated by molecular biological methods (2). Using this cosmid system, called rOka, several VZV-null mutants have been constructed.

One of the mutants was open reading frame 47 (ORF47)-null VZV, designated VZV rOka-47S, in which stop codons replaced codons 166 and 167 of ORF47, the VZV UL protein serine kinase (15). In cell culture, the ORF47-null VZV displayed no distinguishing phenotype with regard to either plaque morphology or growth kinetics. However, VZV rOka-47S could not replicate in fetal skin or thymus implants in SCID-hu mice and replicated less efficiently in human T lymphocytes derived from fetal cord blood, a puzzling development since no tissue culture phenotype was previously observed (27, 40). Thus, ORF47 was required for efficient replication in T lymphocytes but not in tissue culture.

ORF47 resides in the VZV virion tegument, and thus ORF47 enters the cell with the virus during infection (30, 41). A specific in vitro assay has conclusively demonstrated the intrinsic protein kinase activity of ORF47 (20). In vitro, ORF47 phosphorylates IE62, the major VZV transactivator and the main component of the VZV virion tegument (23, 31). Also in vitro, ORF47 phosphorylates and tightly binds ORF63, another resident of the VZV tegument (20, 21).

VZV gE, the predominant viral glycoprotein, is present on the envelope of the mature virion (9). The gE product is a typical type I glycoprotein, which traffics from the ER through the Golgi, where it is extensively processed, to the outer cell membrane. Both the ectodomain and endodomain of gE have important functions. For example, in the ectodomains, a single point mutation in VZV-MSP gE changes VZV MSP egress pattern from a typical "viral highways" phenotype to a diffuse pattern similar to that observed in herpes simplex virus-infected cells (38, 39).

On the infected cell membrane, gE modulates cell-cell spread and syncytium formation (24). At the same time, gE is being internalized. Endocytosis of VZV gE is controlled by two tyrosine-based motifs and an acidic cluster in the cytoplasmic tail. The acidic cluster of gE interacts with phosphofurin acidic cluster sorting protein 1 (PACS-1) and directs VZV gE to the *trans*-Golgi network (TGN), a proposed site of tegument assembly and virion envelopment (1, 4, 35, 44, 51). Phosphorylation within acidic clusters can mediate PACS-1 interaction (6). The gE acidic cluster includes serine and threonine resi-

* Corresponding author. Mailing address: University Hospital/2501 JCP, 200 Hawkins Dr., Iowa City, IA 52242. Phone: (319) 356-2270. Fax: (319) 356-4855. E-mail: charles-grose@uiowa.edu.

dues within a casein kinase II (CKII) consensus sequence beginning at amino acid 591: EDSESTDTEEE (48). VZV gE is known to be phosphorylated on its cytoplasmic tail (11, 28, 33, 48). After observing that the ORF47 phosphorylation consensus sequence required acidic residues, we postulated that the gE acidic cluster might also be phosphorylated by ORF47 (20). Prior experiments showed incorporation of radiophosphate onto VZV gE in both VZV-rOka- and VZV-rOka-47S mutant-infected cells. Other experiments showed that CKII was present in a gE immunoprecipitate (15, 33). Indeed, CKII is ubiquitous, necessary, and especially abundant in cell culture (12, 15, 25, 37, 42). Thus, it may have been difficult to determine the contribution of ORF47 protein kinase in the cellular environment with abundant phosphorylation due to CKII.

To overcome these obstacles, we have reexamined gE phosphorylation under both in vitro and in vivo conditions. The in vivo studies were facilitated by the construction of the ORF47-null virus. The results demonstrate that subtle modifications of gE phosphorylation can dramatically alter both gE trafficking after endocytosis as well as virus cell-cell spread.

MATERIALS AND METHODS

Cells, viruses, and reagents. HeLa (ATCC CCL2) and MeWo cells (10) were grown in Eagle complete medium supplemented with 10% fetal calf serum (GibcoBRL, Rockville, Md.). Construction of VZV rOka and VZV rOka-47S (the ORF47-null mutant) using the VZV cosmid system has been published previously (15). VZV-32 is a low-passage clinical isolate (10). Recombinant vaccinia virus (T7-vaccinia virus) and the expression plasmid pTM1 have been described previously (29). Construction of pTM1-gE containing VZV ORF68 and the point mutations in the acidic cluster have been published (47, 48). The pCAGGS and ORF47.12 systems were described previously (20, 32). The monoclonal antibody (MAb) 3B3 (VZV gE) and the polyclonal antibody R22 (ORF47) have been described elsewhere (13, 30). MAb 158 recognizes full-length VZV gB (24). MAb 5C6 recognizes VZV IE62 (38). MAb 6B5 recognizes VZV gI (49). In the confocal micrographs, all fluorescent-conjugated secondary antibodies, Texas Red-conjugated wheat germ agglutinin (WGA) (Golgi stain), Oregon Green-conjugated phalloidin (actin), and TOTO-3 (nuclear stain) were obtained from Molecular Probes, Portland, Oreg. DRB (5,6-dichlorobenzimidazole riboside) was purchased from Sigma (St. Louis, Mo.).

Coimmunoprecipitation and immunoblotting. At 48 h postinfection (hpi), 75-cm^2 monolayers of MeWo cells infected with VZV-32, VZV rOka, or VZV rOka-47S were lysed in 6 ml of radioimmunoprecipitation buffer with phosphatase and protease inhibitors as previously described (20). HeLa cells were transfected with Lipofectin (GibcoBRL) and lysed as described elsewhere (20). For lysate samples, 300 μl of lysate was reserved and precipitated with cold acetone. For the coimmunoprecipitated samples, MAbs listed under cells and reagents (1:2,000) and protein A-Sepharose precipitated the proteins from 1 ml of lysate. The samples were washed twice in cold lysis buffer and twice with cold kinase buffer (ORF47 kinase buffer [25 mM HEPES, pH 7.4; 50 mM KCl, 10 mM $MnCl_2$] or CKII kinase buffer [50 mM Tris HCl, pH 7.2; 140 mM KCl; 10 mM MgCl]). Lysate or immunoprecipitate separated by sodium dodecyl sulfate (SDS)-polyacrylamide gel electrophoresis and transferred to Hybond ECL nitrocellulose (Amersham Pharmacia, Piscataway, N.J.) and probed according to the manufacturer's protocol (SuperSignal; Pierce, Rockford, Ill.). Each immunoblot was performed three times, and a representative sample is shown.

ORF47 in vitro kinase assays. HeLa cells (5×10^5) were seeded into 35-mm-diameter tissue culture dishes and allowed to adhere overnight at 37°C. For transfections with the pCAGGS plasmid, cells were transfected 18 h later with 4 μg of plasmid DNA per well in a 15% Lipofectin (GibcoBRL) solution in 0.5 ml of Opti-Mem I (GibroBRL). At 3 h posttransfection, 2 ml of fresh medium was added and the cells were incubated overnight at 37°C. For pTM1-gE and mutant gE transfections, HeLa cells were preinfected with recombinant T7-vaccinia virus 1 h before Lipofectin transfection.

At 16 h posttransfection, HeLa cells were pretreated with okadaic acid (Calbiochem, La Jolla, Calif.), lysed in RIPA buffer (0.01 M Tris HCl [pH 7.4], 0.15 M NaCl, 1% NP-40, 1% deoxycholate, 0.1% SDS) with the following phosphatase and protease inhibitors: 50 mM NaF, 1 mM Na_3VO_4, 1 mM phenylmethylsulfonyl fluoride, 1 mM benzamidine, 1 mM leupeptin, and 0.025 trypsin inhibition unit each of aprotinin and I-S soybean trypsin inhibitor. The lysates were incubated for 1 h at 4°C with rotation, scraped into vials, and incubated for another hour with rotation at 4°C. The lysates were sedimented at $35,000 \times g$ for 1 h to remove insoluble material. Lysates from gE or mutant gE samples to be added to ORF47.12 in vitro kinase assays were heated to 80°C for 10 min to inactivate the coprecipitated CKII. Precipitation was carried out with MAb 3B3 and protein A-Sepharose, as the antibody recognizes both the inserted epitope in ORF47.12 and the natural gE 3B3 epitope. The immunoprecipitates were washed twice in cold lysis buffer with the protease and phosphatase inhibitors and twice with cold kinase buffer (ORF47 kinase buffer or CKII kinase buffer).

The in vitro kinase samples were combined with 25 μl of the appropriate kinase buffer to the washed protein A-Sepharose and, when indicated, 1 or 2 μl of a 1-μg/μl heparin solution, 1 μl of a 30 mM solution of spermine (a polyamine necessary for the preservation of the kinase activity of ORF47.12), and the protein A-Sepharose with the immunoprecipitated gE or gE mutant. Radiophosphate (0.5 μCi of [γ-^{32}P]ATP; Amersham) diluted in 4.5 μl of kinase buffer was added to each sample to initiate the kinase reaction. For CKII reactions, CKII kinase buffer was substituted for ORF47 kinase buffer. The samples were reacted for 1 h at 30°C with mixing every 10 min. For supernatant samples, a 30-μl aliquot of the kinase reaction supernatant was removed before washing, precipitated in 80% acetone overnight (−20°C), centrifuged, washed with 80% acetone, and reprecipitated. The kinase reaction in the reaction pellet was halted by adding 1 ml of ice-cold lysis buffer plus inhibitors to the protein A-Sepharose as a first wash. After two washes with lysis buffer and two with kinase buffer, glycerol sample buffer containing 10% beta-mercaptoethanol was added, and the samples were boiled for 5 min.

After washing, the samples were separated by SDS-polyacrylamide gel electrophoresis and radioactivity was quantified by an HP InstantImager and the accompanying software. All data are presented as counts per minute/millimeter^2 − (background counts per minute/millimeter^2) and denoted as counts per minute/millimeter^2 − background. Background was defined as an area of each lane approximately the same size as the experimental band but at 30 kDa, an area in all the gels with little contamination and no protein product for the assays described here. Each kinase assay was performed three times, and a representative sample is shown. The three assays were normalized, and the standard deviation was calculated and renormalized to the example shown in Results.

Confocal microscopy and antibody uptake endocytosis assay. For confocal imaging, at the designated times postinfection, the cells were fixed and permeabilized with 2% paraformaldehyde in Na_2HPO_4 with Triton X-100 (1:2,000) for 1 h. After blocking with 5% milk in phosphate-buffered saline (PBS) (pH 7.4), primary antibodies in PBS and 1% milk were incubated overnight. After washing, the samples were incubated with secondary antibodies conjugated to Alexa fluorescent compounds (1:1,250 in PBS), phalloidin (actin) directly conjugated to Oregon Green (1:300), and TOTO-3, a nucleic acid stain (1:15,000; Molecular Probes, Portland, Oreg.); mounted on microscope slides; and viewed with a Zeiss 510 laser scanning microscope and the accompanying proprietary software. Fluorescence levels were set using the range indicator for each sample, compared to negative and positive controls, and scanned using the multiple track setting.

For the antibody uptake endocytosis assay, at 24 hpi, the live cells were chilled to 4°C for 1 h. The samples were incubated with the indicated primary antibody (all 1:1,000) in Opti-Mem (GibcoBRL) for 1 h at 4°C. In samples treated with DRB, a cell-permeating CKII inhibitor, complete medium containing DRB was added at the indicated concentrations 2 h before the antibody incubation and added back to the samples in complete medium for the indicated time points. Because DRB is diluted in ethanol, an equal amount of ethanol (a total of 9 μl of ethanol in 2 ml of complete medium) was added to all samples as a control. After washing, the live cells in complete medium were returned to 37°C for the indicated times and then fixed and permeabilized as described above. Secondary antibodies and either phalloidin-Oregon Green or WGA (conjugated to Texas Red [1:200; Molecular Probes]) counterstained the actin cytoskeleton or the Golgi bodies, respectively. After nuclear staining, the cells were mounted and viewed as above using the multiple-track setting on the Zeiss 510 confocal laser scanning microscope and the accompanying proprietary software.

In the profile display mode of the proprietary software for the Zeiss 510 laser scanning confocal microscope, the pixel intensities along a selected line can be quantified. Baseline intensity was established using wild-type rOka, and settings remained constant. Immunolabeling was also analyzed by importing the digital images into Photoshop 6.0 and determining the pixel intensity in localized areas by a previously described method (38).

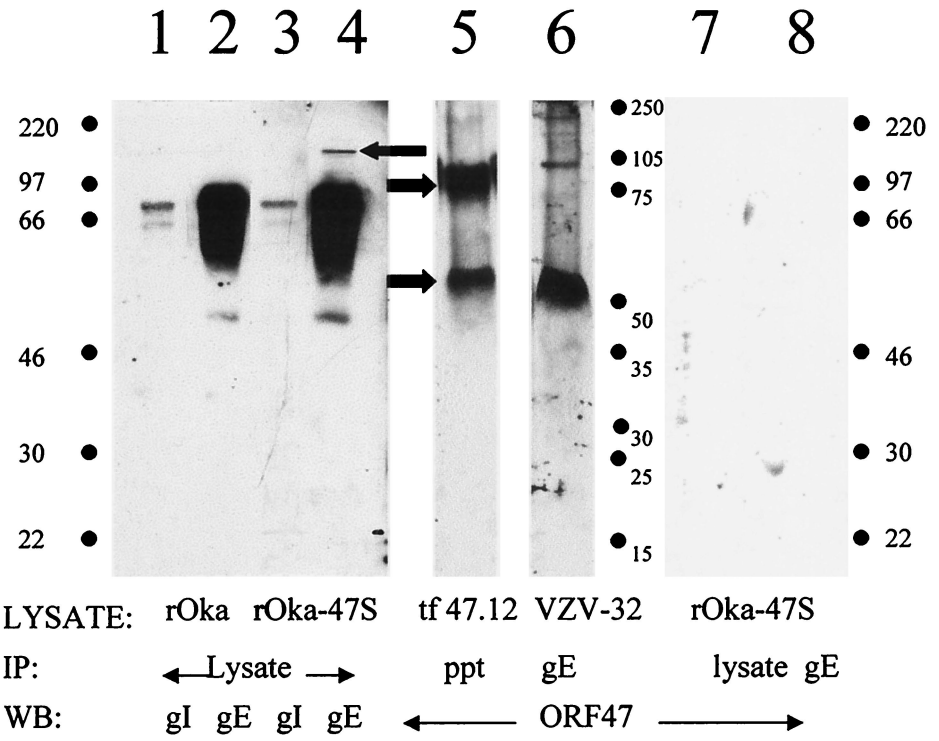

FIG. 1. Detection of gE, gI, and ORF47 in infected cell lysates. Lane 1: wild-type VZV rOka lysate immunoblotted for VZV gI. Lane 2: wild-type VZV rOka lysate immunoblotted for VZV gE. Lane 3: VZV rOka-47S, the ORF47-null mutant, lysate immunoblotted for VZV gI. Lane 4: VZV rOka-47S lysate immunoblotted for VZV gE. Note the VZV gE dimer expressed in rOka-47S (left arrow). Lane 5: ORF47.12 transfected HeLa cell lysate, immunoprecipitated with antibody to the epitope tag, and immunoblotted for ORF47. Note the ORF47.12 monomer (54 kDa) and dimer (110 kDa) (arrows). Lane 6: Coprecipitation of ORF47 with VZV gE from infected cells. VZV-32-infected cell lysate, immunoprecipitated for VZV gE, immunoblotted for ORF47. Both the ORF47 monomer and dimer coprecipitated with VZV gE. Lane 7: rOka-47S lysate immunoblotted for ORF47. Lane 8: rOka-47S lysate immunoprecipitated for VZV gE and immunoblotted for ORF47. Abbreviations: IP, immunoprecipitation; WB, Western blotting, ppt, precipitated total lysate.

RESULTS

Detection of gE, gI, and ORF47 in VZV-infected cells. For purposes of definition, the VZV rOka virus is considered to be wild type, while VZV rOka-47S is the ORF47-null mutant virus. To compare the relative amounts of gE and gI produced in rOka- and rOka-47S-infected cells, we immunoblotted total solubilized lysate from each strain. In the lysate from VZV rOka-infected cells, VZV gI and gE were clearly visible and similar in band density and shape to immunoblots from other VZV isolates (Fig. 1, lanes 1 and 2). In the samples from VZV-rOka-47S lysate, however, the VZV gI appeared normal (lane 3), but an additional band was detected at 150 kDa in the VZV gE sample above the usual 55- to 97-kDa glycoprotein band (lane 4, leftward arrow). This band had the same molecular weight and appearance as an underglycosylated gE dimer that is often found in gE samples purified from transfected cells and from insect cells (33). Thus, a gE dimer existed in VZV-rOka-47S-infected cells that was not found in wild-type VZV-infected cells. As a positive control for ORF47, ORF47.12-transfected HeLa cell lysates were immunoprecipitated and immunoblotted (lane 5). ORF47 was visible as a 54-kDa monomer and as a 110-kDa dimer (rightward arrows). To determine whether ORF47 physically interacts with other viral proteins within infected cells, solubilized VZV-32-infected MeWo cell lysate was immunoprecipitated with MAb to VZV gE. Immunoblotting demonstrated that ORF47 kinase was coprecipitated by VZV gE, both at the expected monomer molecular weight (54 kDa) and as a dimer visible at 110 kDa (lane 6).

As a negative control, VZV rOka-47S lysates were similarly immunoprecipitated and immunoblotted. No ORF47 bands were visible in either the total lysate or the VZV gE lane immunoprecipitated from the mutant VZV rOka-47S lysate (lanes 7 and 8). The latter results confirmed the identity of the immunoblotted band in lane 6. Neither VZV gI nor VZV gB coprecipitated ORF47 from VZV-32-, VZV-rOka-, or VZV-rOka-47S-infected cell lysates (data not shown).

Phosphorylation of VZV gE by ORF47 and CKII. Because ORF47 and CKII share a similar phosphorylation consensus sequence, gE was tested as a substrate in an in vitro kinase assay with each kinase (Fig. 2). Both CKII and ORF47 phosphorylated VZV gE. Addition of 1 mM heparin to the CKII in vitro kinase assay reduced the kinase activity of CKII, while 2 mM heparin reduced CKII-dependent phosphorylation levels to that of background in the vector-only sample. Heparin does not inhibit ORF47 kinase activity (20, 30). Thus, in the ORF47/gE sample with 2 mM heparin. Overall, incorporation of radiophosphate due to ORF47 protein kinase activity was substantially more than the amount of radiophosphate incorporated due to CKII activity.

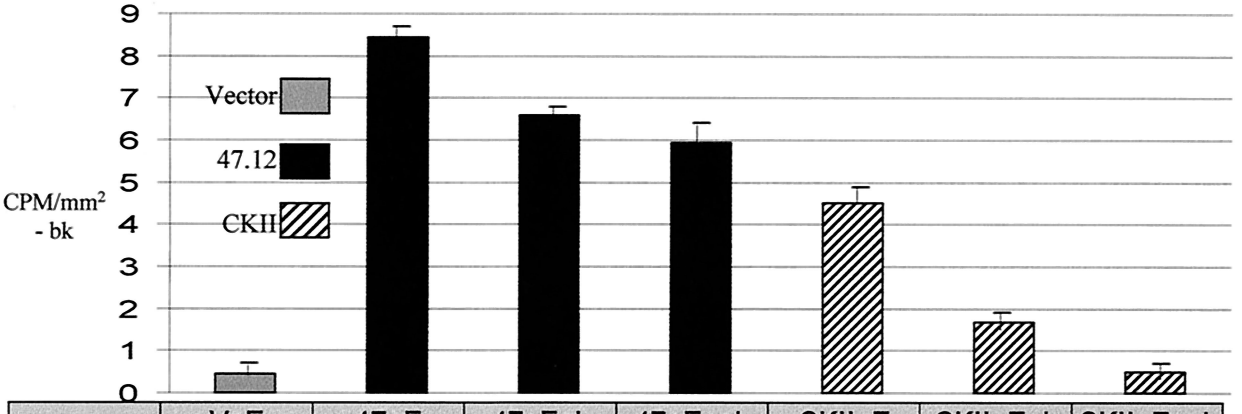

	V+E	47+E	47+E+h	47+E++h	CKII+E	CKII+E+h	CKII+E++h
CPM/mm^2 -	0.455	8.437	6.588	5.94	4.504	1.676	0.508

FIG. 2. Phosphorylation of VZV gE by ORF47 kinase and CKII. Immunoprecipitated VZV gE was added to in vitro kinase assays specific for either ORF47.12 or CKII. Shown are vector-transfected negative control (V+E), ORF47.12 kinase assays with 1 mM (+h) or 2 mM (++h) heparin, and CKII-specific kinase assays with 1 mM (+h) or 2 mM (++h) heparin. This experiment was repeated three times with similarly proportional results, and a representative sample is shown. bk, background. Error bars, standard deviations.

Differential phosphorylation of the gE acidic cluster by ORF47 and CKII. As we postulated that both ORF47 and CKII were phosphorylating VZV gE within the acidic cluster beginning at amino acid 594 (EDSESTDTEEE), we carried out additional kinase assays with previously produced VZV gE constructs with alanine substituting for the four serines or threonines within the acidic cluster (48). ORF47 equally phosphorylated both the initial serines and the trailing threonines in the acidic cluster (Fig. 3). In the analyzed data, approximately equal amounts of radiophosphate were incorporated into the SSAA (EDSESADAEEE) gE and the AATT (EDA EATDTEEE) gE in the ORF47 samples, and these amounts each approximated half the amount of phosphorylation observed in the ORF47/gE wild-type sample. No radiophosphate above background levels was incorporated into the AAAA gE (EDAEAADAEEE) by ORF47. CKII, however, heavily phosphorylated the AATT gE mutant but CKII-dependent phosphorylation of the SSAA gE mutant was reduced. Thus, CKII

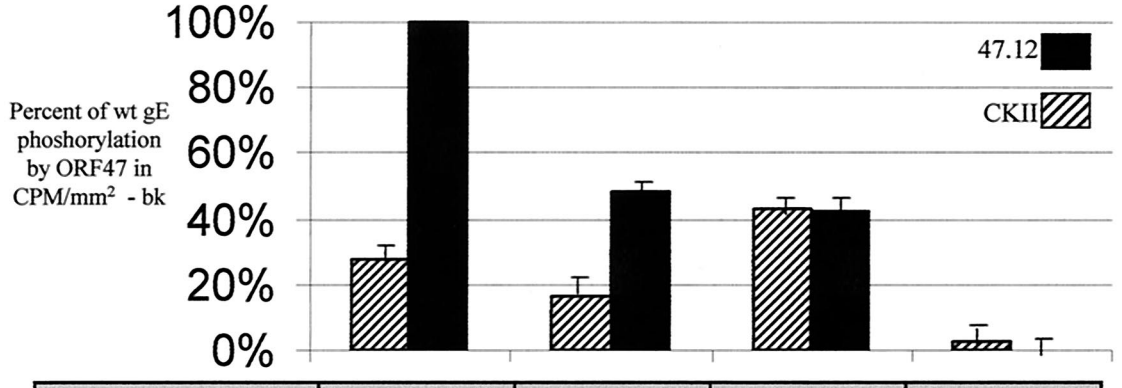

	SSTT gE	SSAA gE	AATT gE	AAAA gE
CKII-bk/47wt	28%	16%	43%	2.30%
47.12-bk/47wt	100%	48%	42%	0%

FIG. 3. Differential phosphorylation of residues within the gE acidic cluster by ORF47 or CKII. The serines and/or threonines in the gE acidic cluster were replaced with alanines, and these point mutants were added to ORF47- or CKII-specific in vitro kinase assays. All ORF47.12 reactions included 2 mM heparin. CKII reactions did not include heparin. Abbreviations: SSTT, wild-type gE (EDSESTDTEEE), SSAA, alanines were substituted for the C-terminal threonines (EDSESADAEEE); AATT, alanines were substituted for the N-terminal serines (EDAEATDTEEE); AAAA, alanines were substituted for all four phosphorylatable residues (EDAEAADAEEE). Note that 47wt indicates the amount of radioactivity incorporated into wild-type gE by ORF47 kinase. This experiment was repeated three times with similarly proportional results, and a representative sample is shown. bk, background. Error bars, standard deviations.

exhibited a marked preference for the two threonine residues, especially when the lower affinity serines were replaced by alanines.

Endocytosis of VZV gE in cells infected with VZV rOka and VZV rOka-47S. Because phosphorylation is known to occur within the acidic domain of gE and because phosphorylation of acidic clusters can affect trafficking to the TGN, we next investigated the trafficking patterns of gE after infection with either wild-type virus or virus lacking a functional ORF47 kinase. MeWo cells, infected with either VZV rOka wild type or VZV rOka-47S, were chilled to halt endocytosis. MAb 3B3, which recognizes an epitope in the extracellular region of VZV gE, was incubated with the cells at 4°C for 1 h. The unbound antibody was washed away and 0-min-time point samples were fixed and permeabilized (Fig. 4A and B). The remaining samples were returned to 37°C to allow endocytosis to occur. At various time points, cells were fixed and permeabilized (time points at 10, 20, 30, and 45 min are not shown; endocytosis after 1 h, Fig. 4C and D). Cells were counterstained with phalloidin (green) for the actin cytoskeleton and TOTO-3 (blue) for the nuclei. Bound gE antibody was visualized with secondary anti-mouse antibodies conjugated to Texas red (red).

At the 0-min time point, antibody-bound gE (red) was found on the plasma membranes of the infected cells and syncytia in both the VZV-rOka-infected MeWo cells (Fig. 4A) and the VZV-rOka-47S-infected MeWo cells (Fig. 4B). The plasma membrane was coincident with an actin ruffle around the perimeter of the cell, here visualized with phalloidin (green). During the intervening time points, VZV gE in VZV rOka-infected MeWo cells relocalized to the center of the syncytia (data not shown). After incubation of VZV rOka-infected cells at 37°C for 1 h., VZV gE (red) endocytosed and was localized in the center of the syncytia within the nuclei ring (blue, Fig. 4C and E). VZV gE endocytosis and relocalization is normally seen in both gE-transfected and VZV-infected cells (35, 51). However, during the intervening time points (data not shown) and after 1 h of incubation in VZV rOka-47S, VZV gE (red) only minimally internalized from the plasma membrane and did not relocalize to the center of the syncytia; instead gE remained on or recycled to the plasma membrane (green, Fig. 4D). VZV gE (red) was retained on or near the plasma membrane of the ORF47-null mutant VZV in both large syncytia (seen at the center of the image) and small syncytia, such as the polykaryon seen on the left of the image.

Using the software accompanying the Zeiss 520 confocal laser scanning microscope, the pixel intensities along a cross-section of the syncytia were analyzed. This software allows the measurement of both pixel intensities and locations. In Fig. 4C and D, the white arrow crossing each syncytium defines the line analyzed in the graph below each micrograph (Fig. 4E and F). In VZV-rOka-infected cells, the center of the syncytia included many bright red pixels, indicating the presence of gE (Fig. 4E). In the VZV rOka-47S-infected cells, however, the center of the syncytia had only a few weakly red pixels, indicating a paucity of gE (Fig. 4F).

Colocalization of internalized VZV gE with the TGN. In VZV-induced fusion, the Golgi bodies from individual cells relocalize to the center of the syncytium, where they are surrounded by the nuclear ring (1, 9, 44). The gE internalization defect observed in the VZV-rOka-47S-infected syncytia may be due to a loss of Golgi stability in the VZV ORF47-null mutant. To recapitulate that VZV gE was sorting to the Golgi in VZV rOka-infected syncytia and to investigate the stability of the Golgi apparatus in VZV-rOka-47S-infected syncytia, WGA conjugated to Texas Red (red) was added to infected, fixed cells after an antibody uptake endocytosis assay (Fig. 5). While WGA strongly stains the TGN, WGA also visualizes the carbohydrates on the plasma and, faintly, nuclear membranes. In both wild-type- and ORF47-null-infected syncytia, the Golgi apparatus relocalized to the centers of the syncytia, as expected (Fig. 5A and B). Colocalization of the Golgi (red) and endocytosed VZV gE (green) was visualized as yellow. After 1 h of incubation, in VZV-rOka-infected syncytia, endocytosed gE colocalized with the Golgi apparatus (Fig. 5A). The Golgi and VZV gE visualized in a globular and punctate distribution (34). However, after 1 h of incubation in VZV-rOka-47S-infected syncytia, VZV gE (green) failed to internalize or colocalize with the Golgi (red), though the Golgi remained intact in the centers of the syncytial nuclear rings (Fig. 5B).

For both 0-min time point samples (VZV rOka and VZV rOka-47S), pixels in the centers of syncytia had very low baseline signal intensity. At the 60-min time point in the VZV-rOka-infected samples, the average pixel intensity increased substantially. It should be noted that abundant amounts of VZV gE relocalized to the Golgi apparatus, which was globular and punctate in micrographs at high resolution. In contrast, in the VZV-rOka-47S-infected cells at the 60-min time point, only a very small amount of VZV gE had reached the centers of the syncytia.

As a control experiment for a global endocytosis defect, we examined the internalization of a second VZV cell-surface glycoprotein, namely, gI, known to contain an endocytosis motif (9, 34). In both wild-type- and mutant-infected cells, gI internalized similarly (Fig. 6). The fact that endocytosis of VZV gI occurred in both the wild-type VZV rOka and the VZV-rOka-47S-infected cells indicated that the ORF47-null mutant did not exhibit a global endocytosis defect. From this result, we inferred that the VZV gE endocytosis defect was specifically related to the lack of ORF47 protein serine kinase activity in the mutant-infected cells.

Effect of inhibition of CKII on VZV gE endocytosis. DRB is a cell-permeating, potent, specific CKII inhibitor. In vitro, 5 μM DRB inhibits CKII kinase activity by 50%, while 45 μM inhibits nearly all CKII kinase activity (50). VZV ORF47 protein kinase was comparatively resistant to DRB in ORF47-specific in vitro kinase assays. When we added DRB to CKII-specific kinase assays at 0, 5, or 45 μM, CKII activity was measured at 100, 50, and 0%, respectively, which agrees with previously published results (3, 50). When DRB was added to ORF47-specific in vitro kinase assays at 0, 5, or 45 μM, ORF47 kinase activity remained at 100, 100, and 70%, respectively.

With the above DRB data, we hypothesized that the addition of DRB to wild-type cells would diminish the CKII contribution and enhance the ORF47 contribution to endocytosis and TGN trafficking. Further, we hypothesized that in mutant virus-infected cells, DRB would inhibit even further the amount of CKII-mediated phosphorylation which contributes to TGN trafficking (as opposed to recycling.) To this end, DRB was added to VZV-rOka-infected cells (Fig. 7A to C) or to

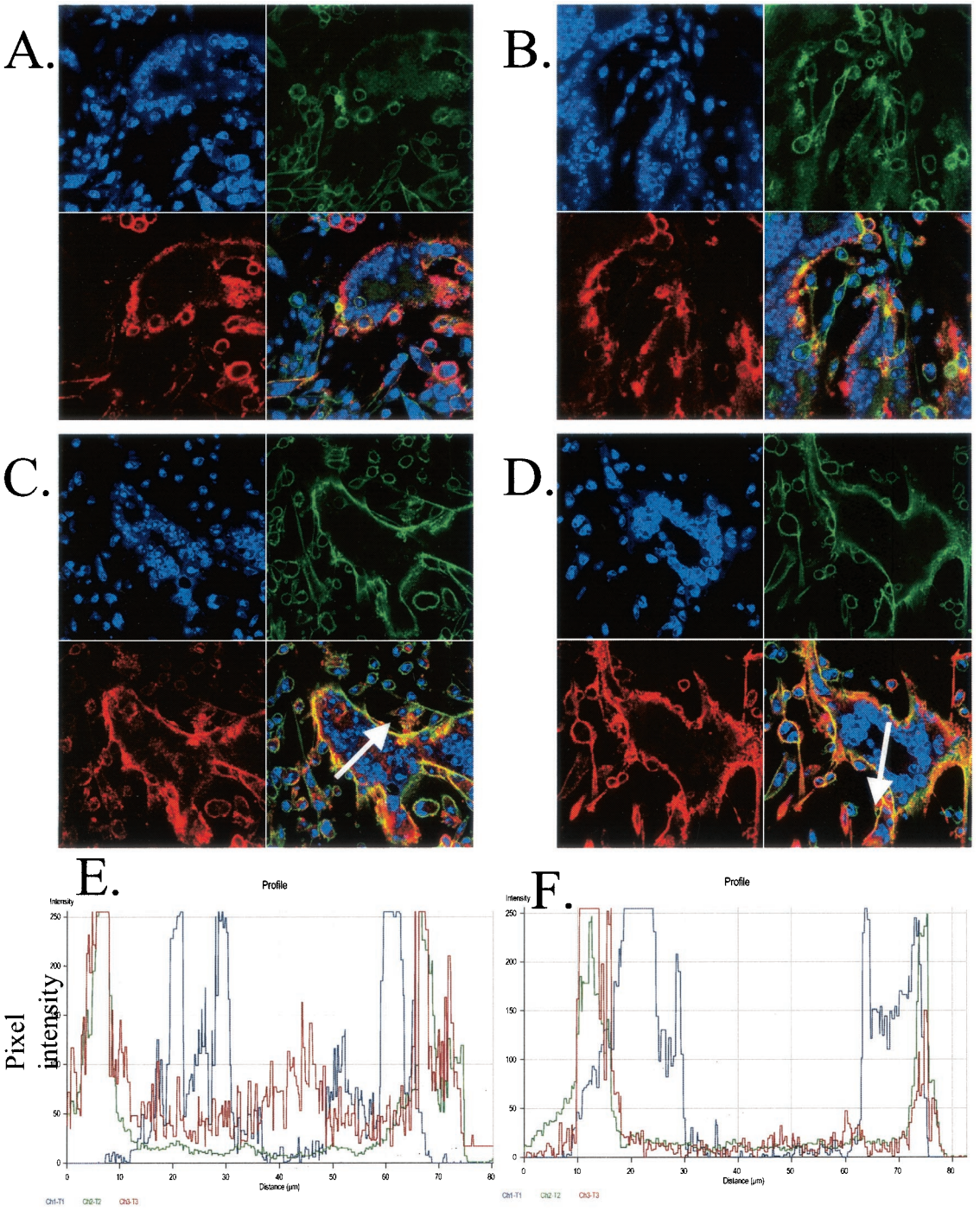

FIG. 4. Endocytosis of VZV gE in cells infected with rOka or rOka-47S. (A, C, and E) rOka-infected cells; (B, D, and F) rOka-47S-infected cells. (A and B) Endocytosis at 0-min time point showing labeled gE (red) on the plasma membrane. Actin (green) was visualized with phalloidin, and the nuclei (blue) were visualized with TOTO-3. (C and D) Endocytosis after 60 min. Note the presence of red in the centers of the syncytia in the rOka sample but not in the centers of the rOka-47S sample. (E and F) Analysis of pixel intensity using the Zeiss software. White arrows in panels C and D overlie the analyzed lines. Note the high levels of red pixel intensity in the rOka sample but not in the rOka-47S sample.

VZV-rOka-47S-infected cells (Fig. 7D to F). Samples were fixed, permeabilized, and processed for confocal microscopy immediately (column 1), after 60 min (column 2), or after 120 min (column 3).

In wild-type VZV-rOka-infected cells, increasing DRB concentration increased the amount of observed VZV gE trafficking to the syncytial centers. In Fig. 7A to C, the amount of VZV gE (red) staining in the centers of each syncytium increased both with increasing DRB concentration and with time. In mutant VZV-rOka-47S-infected cells, increasing DRB

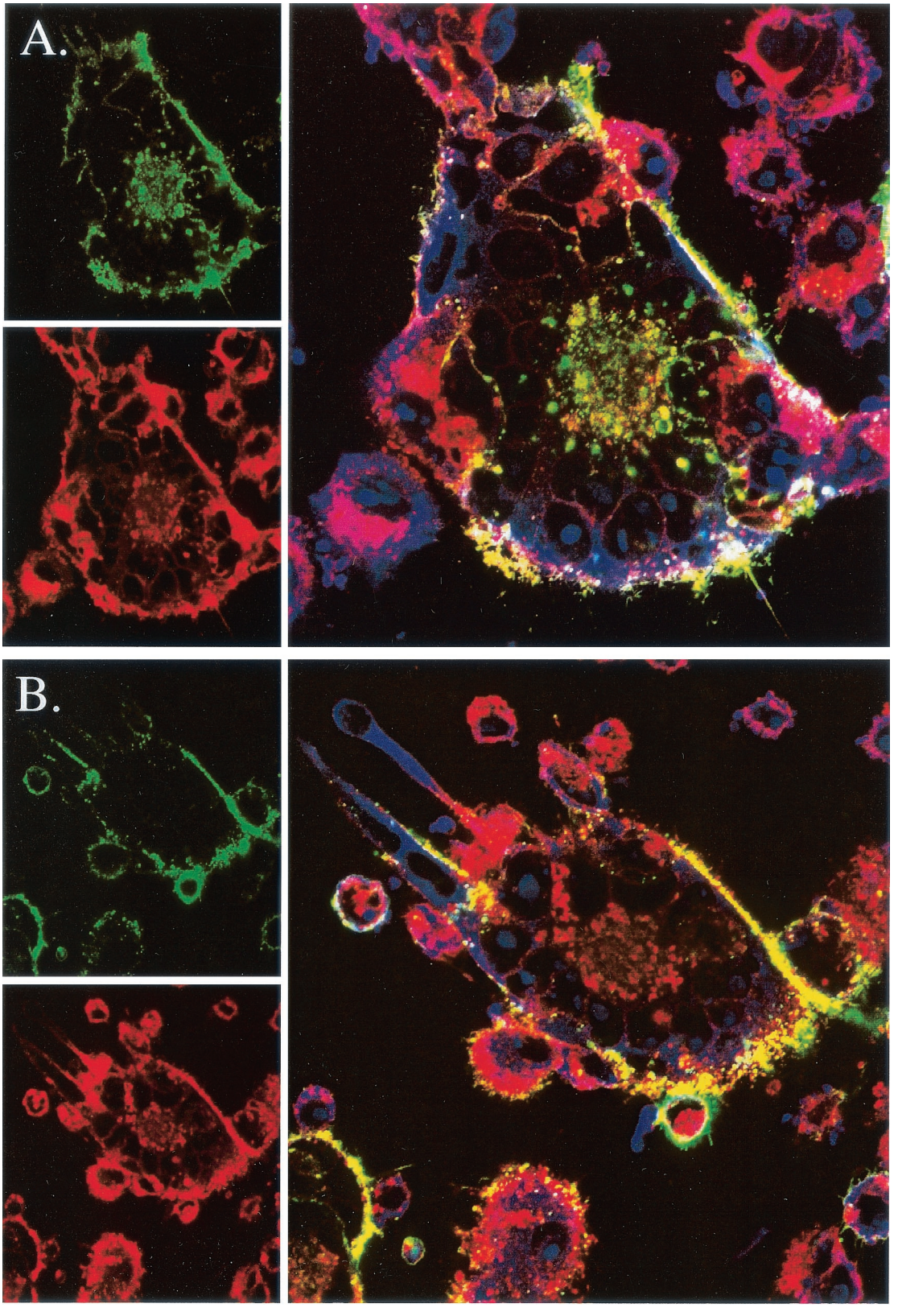

FIG. 5. Localization of endocytosed gE and TGN markers in cells infected with rOka or rOka-47S. Endocytosis of gE was analyzed after 60 min. (A) rOka-infected cells; (B) rOka-47S-infected cells. Individual channels are shown on the left; merged channels are shown on the right. In VZV-infected cells, the TGN (red) relocalizes to the center of the syncytium. Note that gE (green) also relocalized to the TGN (yellow) in rOka-infected cells but not in rOka-47S-infected cells, where the TGN remained a red color.

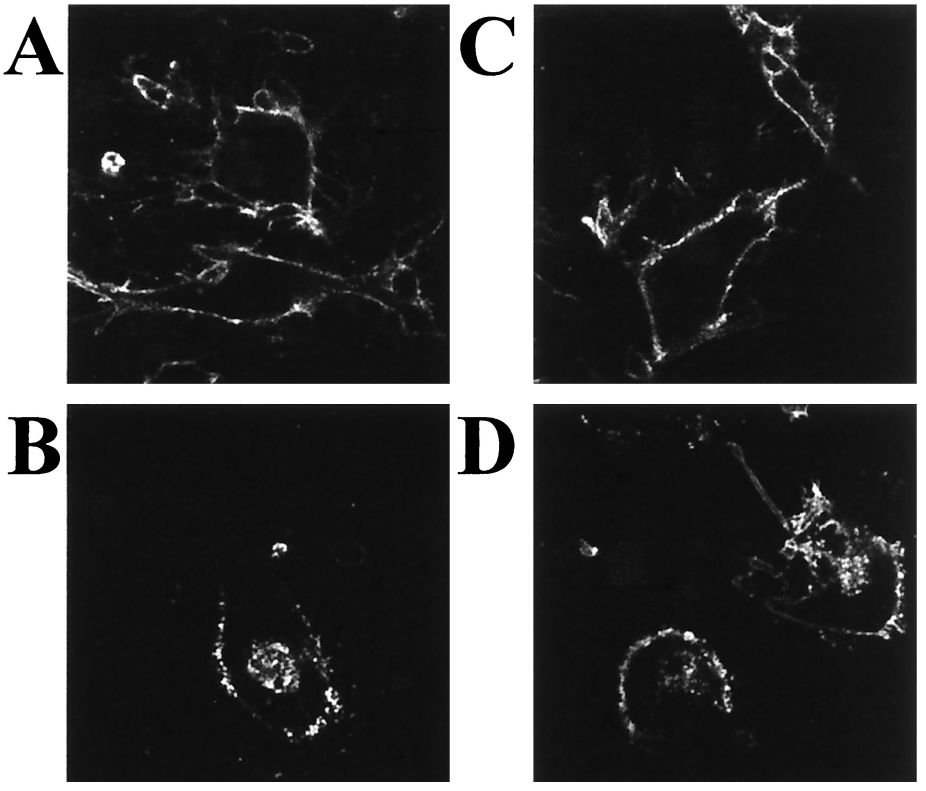

FIG. 6. Endocytosis assay of the VZV gI glycoprotein. (A) VZV rOka, 0 min of endocytosis; (B) VZV rOka, 60 min of endocytosis; (C) VZV rOka-47S, 0 min of endocytosis; (D) VZV rOka-47S, 60 min of endocytosis. Note the signals in the centers of the syncytia in panels B and D.

concentration had the opposite effect on gE trafficking. Relocalization to the TGN of VZV gE decreased with increasing DRB concentration. In the micrographs (Fig. 7D to F), the amount of VZV gE (red) in the centers of the syncytia decreased with the addition of DRB. When the treated samples of both wild-type and mutant cells were compared (Fig. 7C and F, 120-min columns), the diminished relocalization in the mutant-infected cells was even more evident.

Cell-cell spread in cultures infected with VZV rOka and VZV rOka-47S. VZV glycoproteins cause syncytial fusion (5, 24). Decreasing endocytosis of VZV glycoproteins corresponds to increased syncytial formation (16). Thus, the next question addressed the relationship of the increased presence of VZV gE on the infected cell membranes with the rate of VZV cell-cell spread. Replicate samples of MeWo cells were inoculated with synchronized cultures of either wild-type VZV rOka or ORF47-null mutant VZV rOka-47S. At various times after infection (4, 12, 24, and 36 hpi), the samples were processed for confocal microscopy with MAbs to VZV gE, gI, IE62, or ORF33.

We studied the expression of VZV gE and gI in both viral strains because they are excellent indicators of cell-cell spread. Both samples had similar profiles; the gI micrographs are shown in Fig. 8. Since both glycoproteins are expressed as late genes, the signal at the 4-hpi time point indicates residual glycoprotein present in the inoculum. The presence of equal amounts of gI at 4 hpi indicates that equal inocula were added (Fig. 8, column 1). VZV gI was visible on single-infected cells in the wild-type sample at 12 hpi (Fig. 8) and present early on the syncytial plasma membranes and processes in the mutant sample (gI, 12 hpi, 47S; note the large syncytia). The ORF47-null-mutant formed large, irregular syncytia coated with glycoproteins (gI, 24 hpi, 47S) while the wild-type virus produced smaller syncytia and cells beyond the perimeter of the syncytia were negative for gI (gI, 24 hpi, wt). These results showed large, jagged syncytia in the rOka-47S-infected cells earlier than in the wild-type VZV infection.

The second set of data in Fig. 8 show the localization of VZV IE62, the major VZV regulatory protein (36). These IE62 samples provided a comparison of immediate-early protein synthesis between the two VZV strains. At 12 hpi, the VZV-rOka-infected cells showed limited nuclear accumulation of IE62. In the mutant VZV-rOka-47S-infected cells, nuclei positive for IE62 were seen. By 24 hpi, the wild-type VZV-rOka-infected sample had clusters of IE62-positive nuclei, small syncytia. The mutant VZV-rOka-47S-infected sample, however, had formed large syncytia but with fewer nuclei positive for IE62. At 36 hpi, the wild-type VZV-rOka-infected cells formed large syncytia with all nuclei positive for IE62. On the other hand, the mutant VZV-rOka-47S-infected sample formed large, irregularly shaped syncytia that included both IE62-negative nuclei and IE62-positive nuclei. Thus, infection of every nucleus and subsequent IE62 protein production appeared to lag behind gI glycoprotein production in the mutant-infected cells.

The ORF33 serine protease is associated with the immature capsid of VZV (7). At 12 hpi, the distribution of ORF33 was nuclear in both viruses (Fig. 8). At 24 hpi, small syncytia and

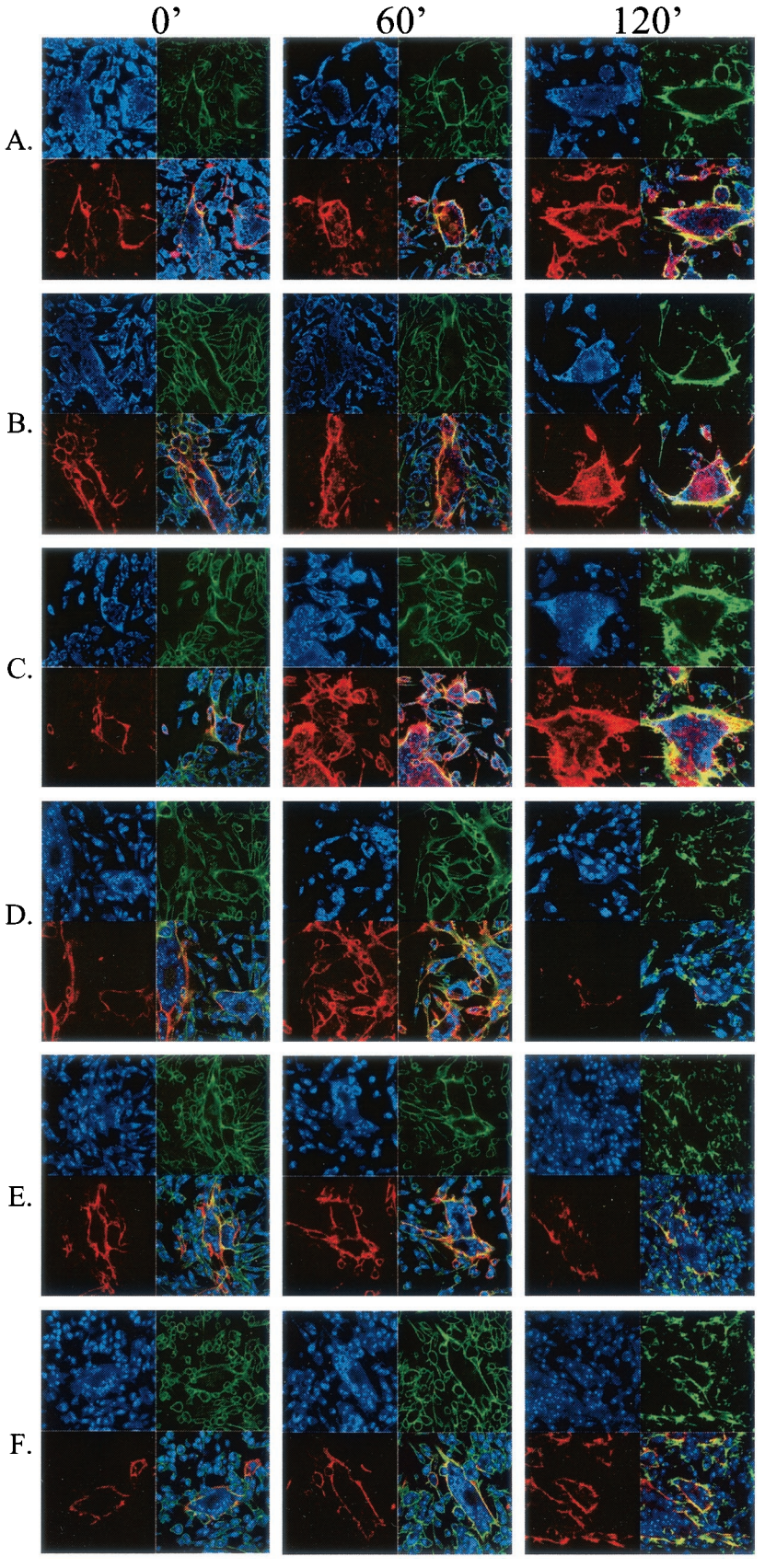

FIG. 7. DRB inhibition of CKII in cells infected with rOka or rOka-47S. Antibody uptake endocytosis assays were performed to investigate the effect of DRB. Red indicates gE endocytosis, green indicates phalloidin staining of the actin cytoskeleton, and blue indicates nuclear stain. Numbers atop the columns indicate duration of endocytosis. (A to C) rOka-infected cells with DRB at 0 (A), 5 (B) or 45 (C) μM. (D to F) rOka-47S-infected cells with DRB at 0 (D) 5 (E), or 45 (F) μM.

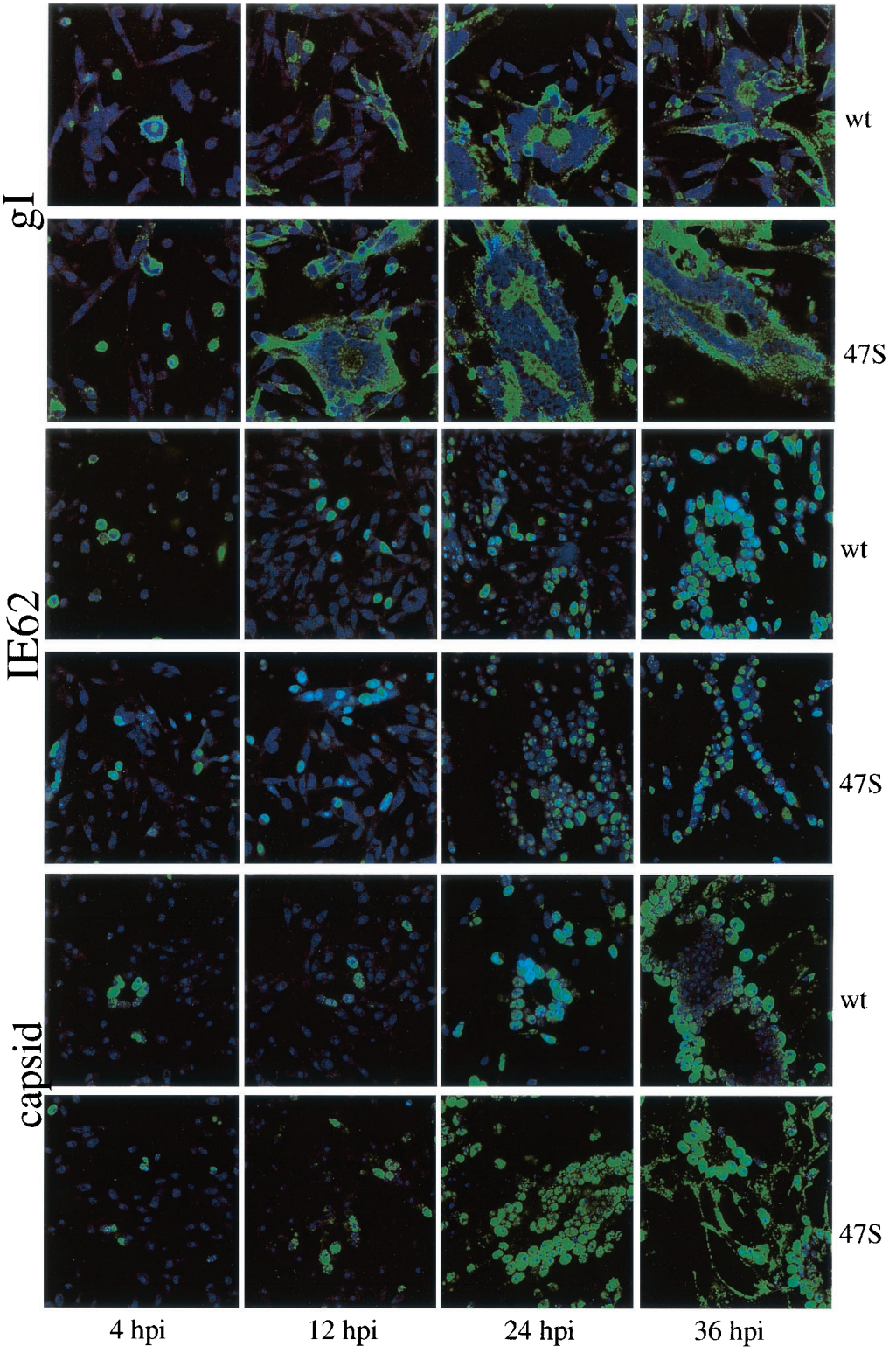

FIG. 8. Differences in cell-to-cell spread between VZV rOka and VZV rOka-47S. Confocal images of VZV-infected cells were analyzed over time. The first, third, and fifth rows show samples infected with VZV rOka (wt). The remaining rows show samples infected with VZV rOka-47S. All viral proteins were visualized as green, and nuclei were visualized as blue. In the top two rows, MAb 6B5 recognizes gI. In the middle two rows, MAb 5C6 recognizes IE62. In the bottom two rows, MAb 251 recognizes the ORF33 serine protease associated with viral capsids.

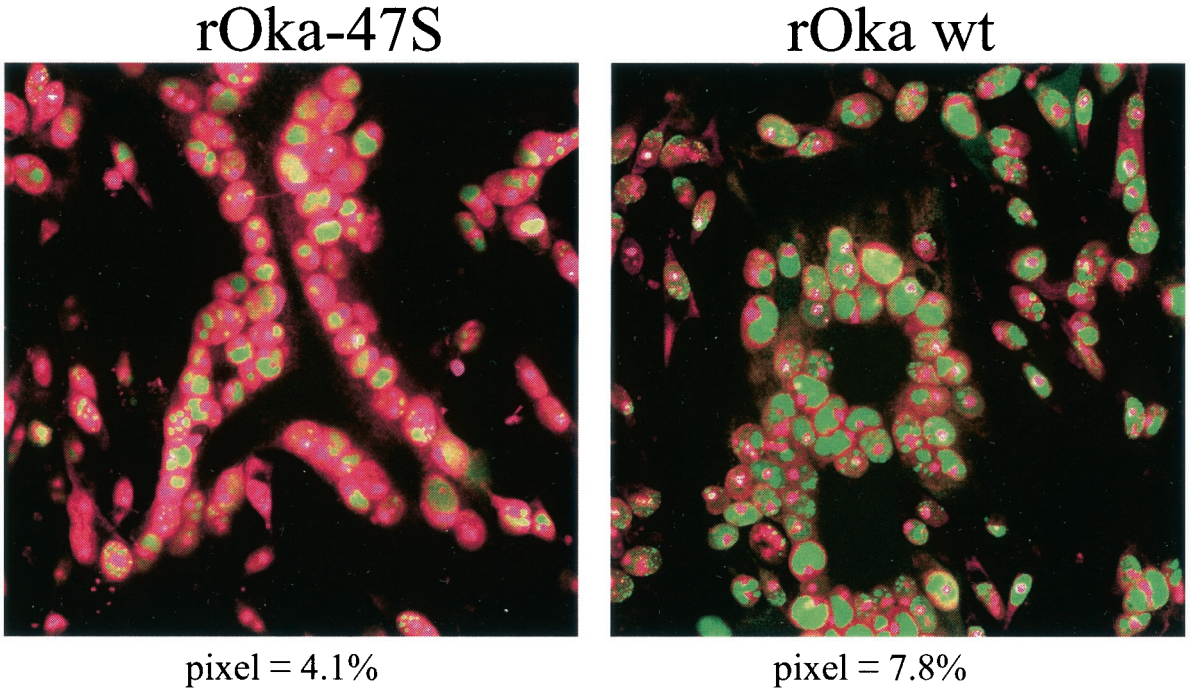

FIG. 9. Identification of VZV IE62 in polykaryons. The 36-hpi micrographs immunolabeled for IE62 shown in Fig. 8 were enlarged in order to better illustrate the differences between cells infected with rOka and rOka-47S. To accentuate the contrast, the nuclei were pseudocolored magenta and the IE62 proteins were colored green. The numbers beneath each micrograph indicate the percentage of IE62 pixels exhibiting the highest intensity, as determined by a previously described assay (38). Note that VZV rOka-47S infection led to the formation of larger, more irregular syncytia, while those of rOka were smaller and circular.

single-infected cells were again visible in the wild-type-infected sample, but larger syncytia were visible in the ORF47-null mutant-infected sample. The larger size of the syncytia was apparent because of the increased ORF33 staining seen in the nuclei of the mutant-infected cells. At 36 hpi in the wild-type sample, the capsid marker exited the nuclei and was found diffusely distributed in the cytoplasm. In contrast, in the ORF47-null mutant-infected sample, the capsid marker relocalized to the rims and processes of the syncytia, which is not a site of virus assembly (8, 44). For clarity, enlargements of two confocal micrographs of VZV IE62 are shown in Fig. 9. Altogether, these imaging results with three different probes showed a more rapid cell spread phenotype in the mutant virus, thus expanding the role of ORF47 protein kinase from gE TGN localization to regulation of VZV cell-cell spread.

DISCUSSION

Regulation of gE localization by phosphorylation. Based on these results, we propose a model for VZV ORF47 regulation of gE localization: either to the Golgi for association with tegument and capsids during virion assembly or to the plasma membrane for cell-cell spread function (Fig. 10). From the plasma membrane, gE is internalized in early endosomes by AP-2 association with the YXXL motif in the endodomain (35, 51). The two protein kinases, the viral ORF47 and the cellular CKII, compete for binding to and phosphorylation of the gE acidic cluster. If ORF47 associates with gE, ORF47 phosphorylates gE equally on the serines in the N-terminal section of the acidic cluster and the threonines in the C-terminal section of the acidic cluster (Fig. 2 and 3). If the N-terminal serines are phosphorylated by ORF47, PACS-1, a sorting protein, binds gE and, by PACS-1-mediated binding to AP-1 and AP-3 adapters, VZV gE is transported to the TGN, a proposed site for tegument association and final envelopment (4, 8, 19, 43). Thus, ORF47 phosphorylation presumably can modify PACS-1 attachment to the gE acidic sequence. If ORF47 phosphorylates the C-terminal threonines of the acidic cluster, then VZV gE is recycled to the plasma membrane. If VZV gE is not associated with ORF47, CKII preferentially phosphorylates the threonines, which biases the gE equilibrium toward recycling and substantially reduces the amount of gE relocalized to the TGN and increases the amount of gE on the plasma membrane. The DRB data presented in Fig. 7 support this model. By inhibiting the CKII pathway with DRB in wild-type rOka-infected cells, kinase competition for gE was reduced and the ORF47 pathway predominated; therefore, more gE relocalized to the TGN, increasing with both time and DRB concentration. In the mutant rOka-47S-infected cells treated with DRB (where gE phosphorylation is exclusively due to CKII), CKII-phosphorylation was reduced and even less gE relocalized to the TGN.

Previously, to support our hypothesis that ORF47 and CKII can phosphorylate consensus sites on different phosphoacceptors, we deduced the ORF47 phosphorylation consensus sequence. Both VZV IE62 and VZV ORF63, along with several other proteins phosphorylated by ORF47, such as maltose-binding protein, the mouse immunoglobulin G2A heavy chain,

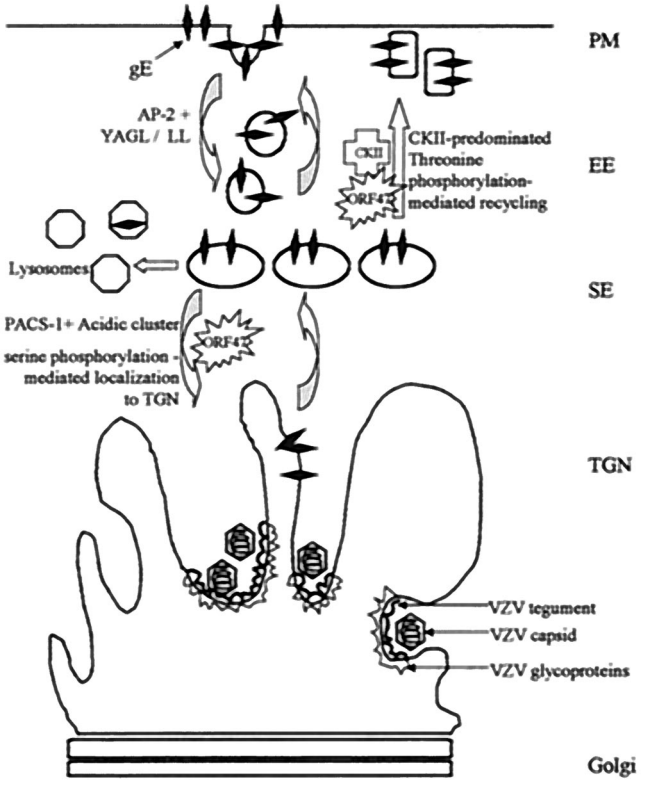

FIG. 10. Effect of phosphorylation by ORF47 kinase and CKII on gE localization. At the plasma membrane (PM), VZV gE associates with and is phosphorylated by either VZV ORF47 or CKII. VZV gE is internalized in early endosomes (EE). If VZV gE is phosphorylated on S593 or S595 (predominantly by ORF47), PACS-1 is postulated to bind the gE acidic cluster in the secondary endosomes (SE) and gE is transported to the TGN. If VZV gE is phosphorylated on T596 or T598 (half the time in ORF47-associated gE, predominantly in CKII-associated gE), PACS-1 is postulated to bind less well and gE recycles back to the plasma membrane.

the rabbit immunoglobulin G heavy chain and casein, include extensive CKII phosphorylation consensus sequences. Three proteins that ORF47 failed to phosphorylate (an ORF62 truncation mutant, glutathione-*S*-transferase, and VZV gB) include no such sequences. CKII phosphorylated VZV gB weakly in vitro. From these data, the ORF47 phosphorylation consensus sequence was deduced: (S/T)X(D/E)(D/E), with a marked preference for additional acidic amino acids in the −1 and +1 position (20). In short, the ORF47 phosphorylation consensus sequence is similar to but more stringent than the CKII phosphorylation consensus sequence, (S/T)XX(D/E) (14).

Effects of ORF47 on viral cell spread phenotype. The results presented in this paper expand concepts about the mechanism of viral cell-cell spread. The gE protein is the major mediator of this property in alphaherpesviruses (18, 24, 26, 38, 46). The two mutually exclusive paradigms are (i) that fully assembled and enveloped capsids pass across plasma membranes and start a new cycle of infection in adjacent cells, and that infection follows the temporal classes of viral protein production, namely, regulatory proteins such as IE62, followed by early proteins such as ORF47, and finally late proteins such as the glycoproteins (18), and (ii) that syncytium formation or other cell-cell spread is not bound by virion assembly processes, but rather that VZV infection proceeds by viral glycoproteins entering uninfected cells and fusing the plasma membranes into syncytia before the appearance of intact virions (22, 24).

The series of confocal micrographs presented in Fig. 8 and 9 show the progression of VZV infection in MeWo cell culture. In the ORF47-null VZV-infected cells, IE62 remained in the nucleus longer than it did in wild-type samples, though the ORF47-null VZV spread faster cell to cell than did the wild type. If fully assembled, enveloped capsids were required for cell-cell spread, IE62 would have been shuttled out of the nucleus for virion assembly sooner in an increased-spread mutant; thus, these data failed to support the first cell-cell spread mechanism detailed above (intact capsids). Besides our results, a separate line of evidence supports the second cell-cell spread mechanism in the absence of virion assembly. Namely, in an ORF66-null VZV mutant, where IE62 is not incorporated into the virion, infectivity continued to spread through the cell culture (17, 22). As also shown in Fig. 8, during late infection of the ORF47-null mutant, the capsid marker (the serine protease associated with the capsids) accumulated at the plasma membrane, which is not a site of virion assembly, but infectivity proceeded and indeed, spread rapidly (44). In wild-type-infected cells, the capsid marker remained in the cytoplasm of the syncytia. These two results provided additional evidence that virion assembly in the rOka-47S-infected cells was disrupted, yet VZV cell-cell spread continued.

Phosphorylation of gE and trafficking in infected cells. In prior publications, we performed phosphoamino acid mapping of gE obtained from virus-infected cells (including both ORF47 and CKII) and gE obtained from transfected cells expressing only CKII. In virus-infected cells, gE is phosphorylated in vivo mainly on serine residues and to a lesser extent on threonine residues (28). In transfected cells (CKII only), we found that CKII phosphorylates gE almost entirely on threonine residues in vivo (48). Results in the present work strongly support our published data, in that we again found that CKII preferentially phosphorylated gE threonines in vitro, while the viral kinase phosphorylated both serine and threonine residues. Considering that gE is predominantly phosphorylated on serines in infected cells (28), we attribute the majority of this phosphorylation to ORF47. Since ORF47-mediated phosphorylation permitted gE translocation to the TGN, the site of viral assembly, we postulate that ORF47-related phosphorylation is of primary importance during infection.

In previous transfection studies, two different endocytic pathways have been proposed as the predominant trafficking pattern for VZV gE. In research conducted in one study, gE expressed in HeLa cells internalized and relocalized to the TGN by colocalization with furin (1). Since these experiments were conducted in transfected cells, no ORF47 or other virally encoded factor was present during the endocytosis of VZV gE. This transfection system was optimized to detect TGN localization of VZV gE, in that an acid strip method removed any external antibody bound to membrane-localized gE and allowed the TGN-localized gE to be observed without distraction. In the in vitro kinase assays presented herein, CKII phosphorylated the serines in the acidic cluster that were associated with TGN localization of gE, albeit with much lower affinity

than did the ORF47 kinase (Fig. 3). Thus, in the above study, low levels of CKII serine-phosphorylated gE localized to the TGN and were detected by the sensitive assay employed.

In a second study, VZV gE expressed in HeLa cells internalized and recycled to the plasma membrane regularly (35). In this study, some internalized gE eventually reached a perinuclear distribution, but colocalization studies with specific TGN markers were not performed. These transfection assays also colocalized gE with the transferrin receptor, which biased the study toward considering the recycling pathway of gE. In recycling assays, in which the glycoproteins trafficked for 30 min, the cells were fixed but not permeabilized, so intracellular gE was not visualized. The first study allowed an hour to elapse during endocytosis, ample time for more gE to be serine phosphorylated and relocalized. In contrast to the above two gE transfection studies, the research in this report was carried out solely with virus-infected cells. The results confirm that VZV gE traffics along both the recycling and the TGN localization pathways. Differential phosphorylation of the EDSESTDT EEE endodomain sequence determines which pathway endocytosed gE follows at each internalization cycle.

ACKNOWLEDGMENTS

T.K.K. thanks the members of the Doctoral Thesis Committee at the University of Iowa for their comments on the data presented in the manuscript.

This research was supported by NIH grants AI22795 and AI36884.

REFERENCES

1. **Alconada, A., U. Bauer, and B. Hoflack.** 1996. A tyrosine-based motif and a casein kinase II phosphorylation site regulate the intracellular trafficking of the varicella-zoster virus glycoprotein I, a protein localized to the trans-Golgi network. EMBO J. **15:**6096–6110.
2. **Cohen, J. I., and K. E. Seidel.** 1993. Generation of varicella-zoster virus (VZV) and viral mutants from cosmid DNAs: VZV thymidylate synthetase is not essential for replication in vitro. Proc. Natl. Acad. Sci. USA **90:**7376–7380.
3. **Critchfield, J. W., J. E. Coligan, T. M. Folks, and S. T. Butera.** 1997. Casein kinase II is a selective target of HIV-1 transcriptional inhibitors. Proc. Natl. Acad. Sci. USA **94:**6110–6115.
4. **Crump, C. M., Y. Xiang, L. Thomas, F. Gu, C. Austin, S. A. Tooze, and G. Thomas.** 2001. PACS-1 binding to adaptors is required for acidic cluster motif-mediated protein traffic. EMBO J. **20:**2191–2201.
5. **Duus, K. M., and C. Grose.** 1996. Multiple regulatory effects of varicella-zoster virus (VZV) gL on trafficking patterns and fusogenic properties of VZV gH. J. Virol. **70:**8961–8971.
6. **Fish, K. N., C. Soderburg-Naucler, and J. A. Nelson.** 1998. Steady-state plasma membrane expression of human cytomegalovirus gB is determined by the phosphorylation state of Ser900. J. Virol. **72:**6657–6664.
7. **Friedrichs, W. E., and C. Grose.** 1986. Varicella-zoster virus p32/p36 complex is present in both the viral capsid and the nuclear matrix of the infected cell. J. Virol. **57:**155–164.
8. **Gershon, A. A., D. L. Sherman, Z. Zhu, C. A. Gabel, R. T. Ambron, and M. D. Gershon.** 1994. Intracellular transport of newly synthesized varicella-zoster virus: final envelopment in the *trans*-Golgi network. J. Virol. **68:**6372–6390.
9. **Grose, C.** 2002. The predominant varicella-zoster virus gE and gI glycoprotein complex, p. 195–224. *In* A. Holzenburg and E. Bogner (ed.), Structure-function relationships of human pathogenic viruses. Kluwer Academic Press, London, United Kingdom.
10. **Grose, C., and P. A. Brunell.** 1978. Varicella-zoster virus: isolation and propogation in human melanoma cells at 36 and 32 degrees C. Infect. Immun. **19:**199–203.
11. **Grose, C., W. Jackson, and J. A. Traugh.** 1989. Phosphorylation of varicella-zoster virus glycoprotein gpI by mammalian casein kinase II and casein kinase I. J. Virol. **63:**3912–3918.
12. **Hanna, D. E., A. Rethinaswamy, and C. V. Glover.** 1995. Casein kinase II is required for cell cycle progression during G_1 and G_2/M in *Saccharomyces cerevisiae*. J. Biol. Chem. **270:**25905–25914.
13. **Hatfield, C., K. M. Duus, D. H. Jones, and C. Grose.** 1997. Epitope mapping and tagging by recombination PCR mutagenesis. BioTechniques **22:**332–337.
14. **Hathaway, G. M., and J. A. Traugh.** 1983. Casein kinase II. Methods Enzymol. **99:**317–331.
15. **Heineman, T. C., and J. I. Cohen.** 1995. The varicella-zoster virus (VZV) open reading frame 47 (ORF47) protein kinase is dispensable for viral replication and is not required for phosphorylation of ORF63 protein, the VZV homolog of herpes simplex virus ICP22. J. Virol. **69:**7367–7370.
16. **Heineman, T. C., and S. L. Hall.** 2002. Role of varicella-zoster virus gE cytoplasmic domain in gB transport and viral egress. J. Virol. **76:**591–599.
17. **Heineman, T. C., K. Seidel, and J. I. Cohen.** 1996. The varicella-zoster virus ORF66 protein induces kinase activity and is dispensable for viral replication. J. Virol. **70:**7312–7317.
18. **Johnson, D. C., M. Webb, T. W. Wisner, and C. Brunetti.** 2001. Herpes simplex virus gE/gI sorts nascent virions to epithelial cell junctions, promoting virus spread. J. Virol. **75:**821–833.
19. **Jones, F., and C. Grose.** 1988. Role of cytoplasmic vacuoles in varicella-zoster virus glycoprotein trafficking and virion envelopment. J. Virol. **62:**2701–2711.
20. **Kenyon, T., J. Lynch, J. Hay, W. Ruyechan, and C. Grose.** 2001. Varicella-zoster virus ORF47 protein serine kinase: characterization of a cloned, biologically active phosphotransferase and two viral substrates, ORF62 and ORF63. J. Virol. **75:**8854–8858.
21. **Kinchington, P. R., D. Bookey, and S. E. Turse.** 1995. The transcriptional regulatory proteins encoded by varicella-zoster open reading frames (ORFs) 4 and 63, but not ORF61, are associated with purified virus particles. J. Virol. **69:**4274–4282.
22. **Kinchington, P. R., K. Fite, A. Seman, and S. E. Turse.** 2001. Virion association of IE62, the varicella-zoster virus (VZV) major transcriptional regulatory protein, requires expression of the VZV open reading frame 66 protein kinase. J. Virol. **75:**9106–9113.
23. **Kinchington, P. R., J. Hougland, A. Arvin, W. Ruyechan, and J. Hay.** 1992. The varicella-zoster virus immediate-early protein IE62 is a major component of virus particles. J. Virol. **66:**359–366.
24. **Maresova, L., T. J. Pasieka, and C. Grose.** 2001. Varicella-zoster virus gB and gE coexpression, but not gB or gE alone, leads to abundant fusion and syncytium formation equivalent to those from gH and gL coexpression. J. Virol. **75:**9483–9492.
25. **Marshak, D. R., and G. L. Russo.** 1994. Regulation of protein kinase CKII during the cell division cycle. Cell. Mol. Biol. Res. **40:**513–517.
26. **Mo, C., E. E. Schneeberger, and A. M. Arvin.** 2000. Glycoprotein E of varicella-zoster virus enhances cell-cell contact in polarized epithelial cells. J. Virol. **74:**11377–11387.
27. **Moffat, J. F., L. Zerboni, M. H. Sommer, T. C. Heineman, J. I. Cohen, H. Kaneshima, and A. M. Arvin.** 1998. The ORF47 and ORF66 putative protein kinases of varicella-zoster virus determine tropism for human T cells and skin in the SCID-hu mouse. Proc. Natl. Acad. Sci. USA **95:**11969–11974.
28. **Montalvo, E. A., and C. Grose.** 1986. Varicella zoster virus glycoprotein gpI is selectively phosphorylated by a virus-induced protein kinase. Proc. Natl. Acad. Sci. USA **83:**8967–8971.
29. **Moss, B., O. Elroy-Stein, T. Mijukani, W. A. Alexander, and T. R. Fuerst.** 1990. New mammalian expression vector. Nature (London) **348:**91–92.
30. **Ng, T. I., and C. Grose.** 1992. Serine protein kinase associated with varicella-zoster virus ORF47. Virology **191:**9–18.
31. **Ng, T. I., L. Keenan, P. R. Kinchington, and C. Grose.** 1994. Phosphorylation of varicella-zoster open reading frame (ORF) 62 regulatory gene product by viral ORF47-associated protein kinase. J. Virol. **68:**1350–1359.
32. **Niwa, H., K. Yamamura, and J. Miyazaki.** 1991. Efficient selection for high-expression transfectants with a novel eukaryotic vector. Gene **108:**193–200.
33. **Olson, J. K., G. A. Bishop, and C. Grose.** 1997. Varicella-zoster virus Fc receptor gE glycoprotein: serine/threonine and tyrosine phosphorylation of monomeric and dimeric forms. J. Virol. **71:**110–119.
34. **Olson, J. K., and C. Grose.** 1998. Complex formation facilitates endocytosis of the varicella-zoster virus gE:gI Fc receptor. J. Virol. **72:**1542–1551.
35. **Olson, J. K., and C. Grose.** 1997. Endocytosis and recycling of varicella-zoster virus Fc receptor glycoprotein gE: internalization mediated by a YXXL motif in the cytoplasmic tail. J. Virol. **71:**4042–4054.
36. **Perera, L. P., J. D. Mosca, W. T. Ruyechan, G. S. Hayward, S. E. Straus, and J. Hay.** 1993. A major transactivator of varicella-zoster virus, the immediate-early protein IE62, contains a potent N-terminal activation domain. J. Virol. **67:**4474–4483.
37. **Prowald, K., H. Fischer, and O. G. Issinger.** 1984. Enhanced casein kinase II activity in human tumor cell cultures. FEBS Lett. **176:**479–483.
38. **Santos, R. A., C. C. Hatfield, N. L. Cole, J. A. Padilla, J. F. Moffat, A. M. Arvin, W. T. Ruyechan, J. Hay, and C. Grose.** 2000. Varicella-zoster virus gE escape mutant VZV-MSP exhibits an accelerated cell-to-cell spread phenotype in both infected cell cultures and SCID-hu mice. Virology **275:**306–317.
39. **Santos, R. A., J. A. Padilla, C. Hatfield, and C. Grose.** 1998. Antigenic variation of varicella-zoster virus Fc receptor gE: loss of a major B cell epitope in the ectodomain. Virology **249:**21–31.
40. **Soong, W., J. C. Schultz, A. C. Patera, M. H. Sommer, and J. I. Cohen.** 2000. Infection of human T lymphocytes with varicella-zoster virus: an analysis with viral mutants and clinical isolates. J. Virol. **74:**1864–1870.
41. **Stevenson, D., K. L. Colman, and A. J. Davison.** 1994. Characterization of the putative protein kinases specified by varicella-zoster virus genes 47 and 66. J. Gen. Virol. **75:**317–326.
42. **Tuazon, P. T., and J. A. Traugh.** 1991. Casein kinase I and II—multipotential

serine protein kinases: structure, function, and regulation. Adv. Second Messenger Phosphoprotein Res. **23:**123–164.

43. **Wan, L., S. Molloy, L. Thomas, G. Liu, Y. Xiang, S. Rybak, and G. Thomas.** 1998. PACS-1 defines a novel gene family of cytosolic sorting proteins required for trans-Golgi network localization. Cell **94:**205–216.
44. **Wang, Z., M. D. Gershon, O. Lungu, Z. Zhu, S. Mallory, A. M. Arvin, and A. A. Gershon.** 2001. Essential role played by the C-terminal domain of glycoprotein I in envelopment of varicella-zoster virus in the *trans*-Golgi network: interactions of glycoproteins with tegument. J. Virol. **75:**323–340.
45. **Weller, T. H.** 1953. Serial propagation in vitro of agents producing inclusion bodies derived from varicella and herpes zoster. Proc. Soc. Exp. Biol. Med. **83:**340–346.
46. **Wisner, T., C. Brunetti, K. Dingwell, and D. C. Johnson.** 2000. The extracellular domain of herpes simplex virus gE is sufficient for accumulation at cell junctions but not for cell-to-cell spread. J. Virol. **74:**2278–2287.
47. **Yao, Z., D. H. Jones, and C. Grose.** 1992. Site-directed mutagenesis of herpesvirus glycoprotein phosphorylation sites by recombination polymerase chain reaction. PCR Methods Appl. **1:**205–207.
48. **Yao, Z., W. Jackson, and C. Grose.** 1993. Identification of the phosphorylation sequence in the cytoplasmic tail of the varicella-zoster Fc receptor glycoprotein gpI. J. Virol. **67:**4464–4473.
49. **Ye, M., K. M. Duus, J. Peng, D. H. Price, and C. Grose.** 1999. Varicella-zoster virus Fc receptor component gI is phosphorylated on its endodomain by a cyclin-dependant kinase. J. Virol. **73:**1320–1330.
50. **Zandomeni, R., and R. Weinmann.** 1984. Inhibitory effect of 5,6-dichloro-1-β-D-ribofuranosylbenzimidazole on a protein kinase. J. Biol. Chem. **259:** 14804–14811.
51. **Zhu, Z., Y. Hao, M. D. Gershon, R. T. Ambron, and A. A. Gershon.** 1996. Targeting of glycoprotein I (gE) of varicella-zoster virus to the *trans*-Golgi network by an AYRV sequence and an acidic amino acid-rich patch in the cytosolic domain of the molecule. J. Virol. **70:**6563–6575.